Research Article | Vol. 10, No. 2 | 1 Feb 2019 | BIOMEDICAL OPTICS EXPRESS 487
Biomedical Optics EXPRESS

Deep UV dispersion and absorption spectroscopy of biomolecules

SOHEIL SOLTANI, ASHKAN OJAGHI, AND FRANCISCO E. ROBLES*

Wallace H. Coulter Dept. of Biomedical Engineering, Georgia Institute of Technology and Emory University, 313 Ferst Dr. NW, Atlanta, GA 30332, USA
**robles@gatech.edu*

Abstract: Owing to the high precision and sensitivity of optical systems, there is an increasing demand for optical methods that quantitatively characterize the physical and chemical properties of biological samples. Information extracted from such quantitative methods, through phase and/or amplitude variations of light, can be crucial in the diagnosis, treatment and study of disease. In this work we apply a recently developed quantitative method, called ultraviolet hyperspectral interferometry (UHI), to characterize the dispersion and absorbing properties of various important biomolecules. Our system consists of (1) a broadband light source that spans from the deep-UV to the visible region of the spectrum, and (2) a Mach–Zehnder interferometer to gain access to complex optical properties. We apply this method to characterize (and tabulate) the dispersive and absorptive properties of hemoglobin, beta nicotinamide adenine dinucleotide (NAD), flavin adenine dinucleotide (FAD), elastin, collagen, cytochrome c, tryptophan and DNA. Our results shed new light on the complex properties of important biomolecules.

1. Introduction

There is an increasing interest in analyzing both the absorptive and dispersive optical properties of biological samples in order to gain a more detailed understanding of their physical and chemical composition for basic research and the study of disease [1–6]. (Dispersion refers to changes in the real part of the refractive index as a function of wavelength). While there are numerous studies that have applied interferometry to study such complex spectral properties in cells and tissues, nearly all of them operate in the visible region of the spectrum [7–15] which has limited endogenous molecular targets (namely hemoglobin and melanin). The UV region (200-400 nm), on the other hand, can provide much more specific molecular insight given that many endogenous molecules interact strongly with light in this spectral range.

In this work we present, to the best of our knowledge, the first study of the unique absorptive *and* dispersive signatures of several physiologically important biomolecules in the deep-UV region of the spectrum. Our approach is based on a recently developed ultraviolet hyperspectral interferometry (UHI) setup [1], which enables deep-UV, wide-band, high-resolution, and high sensitivity spectroscopic measurements of the refractive index and molar extinction coefficient of biomolecules. UHI microscopy was developed to provide quantitative spectral information of endogenous molecules with subcellular spatial resolution and sensitivity to nanometer-scaled structures for label-free molecular imaging of live cells and thin tissue samples [1]. In this work we analyze the deep-UV absorptive and dispersive properties of biomolecules that play an important role in the structure and function of biological systems to gain a better understanding of their spectral properties. Measured molecules include hemoglobin, beta nicotinamide adenine dinucleotide (NAD), flavin adenine dinucleotide (FAD), elastin, collagen, cytochrome c, tryptophan and DNA. Results show the capabilities of this method to quantify the deep-UV complex spectral signatures of the aforementioned biomolecules at physiologically relevant concentrations. This work has

#347919 https://doi.org/10.1364/BOE.10.000487
Journal © 2019 Received 12 Oct 2018; revised 7 Dec 2018; accepted 9 Dec 2018; published 8 Jan 2019

Biomedical Optics EXPRESS

important implications not only for UHI microscopy and other dispersion-based imaging systems, but also for the broader spectroscopy community given that most (UV) spectroscopic measurements of biomolecules have focused on absorptive or fluorescent properties, while dispersive features have been largely neglected [15–25].

2. Methods and materials

2.1 Optical setup

The optical system (Fig. 1) is designed based on a Mach-Zehnder interferometry configuration, consisting of a broadband laser-driven plasma light source (Eq. (-99)X LDLS, Energetiq Technology). A set of off-axis parabolic mirrors (Newport Corporation) are used to collimate the output light. Then, the incoming broadband optical beam is divided into two equal beams, one of which is used as reference and only carries free-space propagation phase accumulation. The second beam passes through the sample and picks up additional wavelength-dependent phase delays based on the optical pathlength difference (OPL) that is proportional to the thickness and refractive index of the sample under test. The sample beam also undergoes attenuation. The resulting wideband interference signal is recorded using an imaging spectrometer (IsoPlane-160, Princeton Instruments) equipped with a high-speed back-illuminated sCMOS camera (Kuro 1200, Princeton Instruments) which has enhanced quantum efficiency in the deep UV range. Here, data are recorded in the form of a 1200 × 1200-pixel image by the sCMOS camera which is a function of wavelength along the columns, and spatial dimension across the rows of the camera (see Fig. 2).

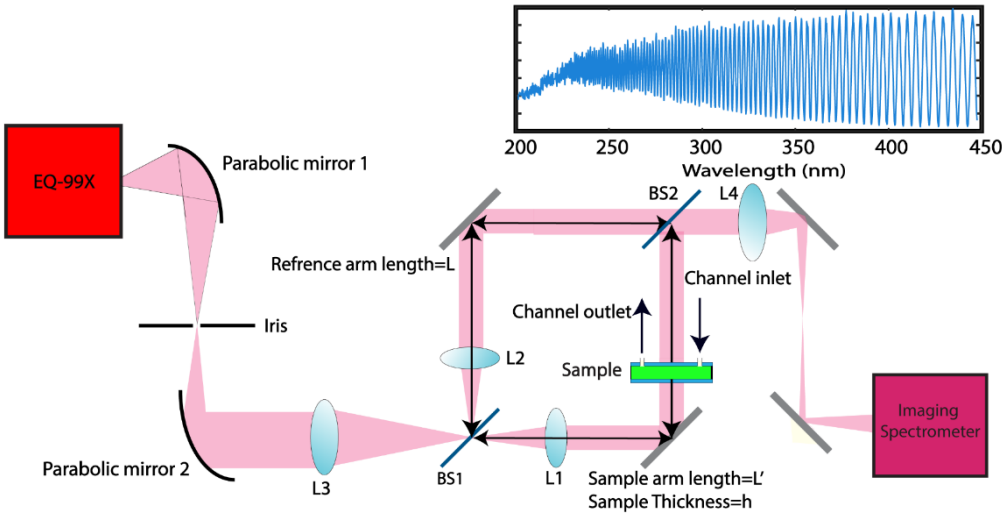

Fig. 1. Schematic of interferometric setup. The incoming light is split into a sample and reference arm. The sample beam passes through a short path length flow cell (in green) and picks up a differential optical pathlength with respect to the reference arm. The inset shows a representative interferogram (intensity vs wavelength).

To test the biomaterials, it is crucial that the sample thickness remain constant throughout the experiment. To this end, dissolved samples are placed in a quartz, short path length flow cell (Spectrosil 49-Q-0.2, Starna Cells) which enables us to acquire measurements from a fixed point while injecting different solutions through the channel inlet. This way, the measured thickness remains constant, plus we avoid any sample movement, improving the reliability of the measurements. The thickness of the sample is 220 microns, and the total optical power on sample arm is 3.35 mW with a beam diameter of 1.3 mm.

Biomedical Optics EXPRESS

2.2 Materials

The specific samples tested in this work were chosen because they play an important role in cellular structure and function. To ensure stability of materials and reproducibility of the experiments we used commercially available biomolecules. Table 1 outlines the specific materials, followed by a brief summary of their importance. These materials are dissolved in deionized (DI) water, except collagen which was dissolved in a 0.1 mM acetic acid solution.

Table 1. list of characterized biomaterials

Material name	Concentration (gr/L)	Sigma-Aldrich Catalog number
Human Hemoglobin (unstabilized Hb)	2	H7379-1G
β-Nicotinamide adenine dinucleotide (βNAD)	0.5	N0632-5G
Flavin adenine dinucleotide disodium salt hydrate FAD)	0.5	F6625-100MG
Elastin,soluble from bovine neck ligament salt-free, lyophilized powder (ELAS)	3	E6527-1G
Hemoglobin Ferrous stabilized (St-Hb)	5	H0267-25MG
DNA from Calf thymus (Calf DNA)	1	D4522-5MG
Cytochrome c from bovine heart (Cyt C)	2	C2037-100MG
Tryptophan (Tryp)	0.5	PHR1176-1G
Collagen from rat tail (Col)	1	C7661-50MG

Hemoglobin: Hemoglobin is an oxygen carrying heterotetramer with globin subunits each attached to a heme group. The main role of Hemoglobin is to carry Oxygen from lungs to tissues and remove CO_2 from tissues to lungs [26].

βNAD: Nicotinamide adenine dinucleotide is a coenzyme that aids in redox process of molecules. This coenzyme accepts electrons from one reaction and becomes reduced which can then deliver electron to another reaction and therefore aids in energy production in cells [27,28].

FAD: Similar to βNAD, FAD is also a redox protein. FAD has 4 states that enables it to accept or deliver electrons hydrogen atoms, or hydronium ions by converting among these states [29,30].

Elastin: Elastin a matrix protein that provides the tissues with elasticity and resilience. It is roughly 1000 times more flexible than the collagens and therefore it is present in lungs, skin and veins [31].

Cytochrome c: The main role of Cytochrome c is electron transfer in mitochondria. Cytochrome c receives electrons from bc_1-complex (cytochrome *c* – oxidoreductase) and transfers it to the complex IV (cytochrome c oxidase). In addition, Cytochrome c plays an important role in cell apoptosis [32,33].

Calf thymus DNA: DNA extracted from calf thymus is an abundant source of high molecular weight pure DNA to study properties and interactions of DNA. One of the main applications of calf DNA is to study DNA binding anticancer agents [34–36].

Tryptophan: Is a type of essential amino-acid that aids in biosynthesis of some necessary complex proteins in human body. It is a precursor for serotonin and melatonin that have direct effect on mental health and sleep patterns [37,38].

Collagen: Collagen is the most abundant protein in human body. It is mostly used in connective tissues and has a varying level of rigidity. It is mostly found in ligaments, skin, vessels and teeth [39–42].

Biomedical Optics EXPRESS

3. Theory and data analysis

To extract the concentration independent refractive index increment, B(λ), and molar extinction coefficient, ε(λ)—two important intrinsic parameters of biological materials—we rely on the interference between the sample and reference fields (see Fig. 1). Phase and intensity difference as a function of wavelength produced by the various samples compared to their solvent allows us to measure these two properties independently. ε(λ) is a measure of optical absorption of the sample per unit length in one mole of material; i.e., a concentration and pathlength independent measure of absorption. Similarly, B(λ) indicates how much the refractive index of the sample changes as a function of wavelength, independent of concentration.

Assuming that the incoming field is split into two, denoted as E_s and E_r, where E_s passes through an absorptive and dispersive medium of interest, then at the point where the two beams interfere the total field is given by:

$$E(\lambda)_{tot} = E_r(\lambda)\exp(-jkL) + \exp(-\frac{\mu_a h}{2})E_s(\lambda)\exp(-jk(L'-h) - jkn(\lambda)h) \quad (1)$$

where $k = 2\pi/\lambda$ is the wavenumber, λ is the wavelength, n is the refractive index, μ_a is the absorption coefficient, $j\sqrt{-1}$, L and L' are the reference and sample arm lengths, and h is the sample thickness (Fig. 1 illustrates *L, L' and h*). Thus, the intensity, $I_{tot} = E_{tot} \times E^*_{tot}$, can be expressed as,

$$\begin{aligned} I(\lambda)_{tot} &= \exp(-\mu_a h)E_s(\lambda)^2 + E_r(\lambda)^2 \\ &+2\exp(-\frac{\mu_a h}{2})E_r(\lambda)E_s(\lambda)\cos(k(L'-L) + kh(n(\lambda)-1)) \end{aligned} \quad (2)$$

The final signal has two main components, a DC component that is proportional to the sample and reference field amplitudes and a sinusoidal term that contains two phase arguments. The first phase argument depends on a constant optical pathlength difference between two arms and linearly depends on k, carrying no information about the sample properties, while the second term depends on the thickness, h, and refractive index of the sample. To remove the DC terms and the first phase term, we take another measurement with only the solvent solution (e.g., DI water) as well as independent measurements of the sample and reference arms for background subtraction. Finally, we subtract the phase term of the solvent measurement from the solution under test which yields,

$$\Delta\varphi(\lambda) = \Delta OPL(\lambda)\,2\pi/\lambda = h(n_{samp}(\lambda) - n_{solv}(\lambda))\,2\pi/\lambda \quad (3)$$

where $n_{samp}(\lambda)$ and $n_{solv}(\lambda)$ are the wavelength-dependent refractive indices of the sample and solvent, respectively. ΔOPL refers to optical pathlength difference between sample and reference arms. Since we have made our sample solution using the same solvent, the refractive index of the sample solution equals:

$$n_{samp}(\lambda) = n_{solv}(\lambda) + B(\lambda)c \quad (4)$$

where B(λ) is the refractive index increment, which is a concentration-independent, intrinsic property of the biomaterial, and c is its concentration in the solution. Thus Eq. (3) simplifies to:

$$\Delta OPL(\lambda) = hB(\lambda)c \quad (5)$$

which directly yields B(λ).

Figure 2 illustrates the interferometric data described by Eq. (2), as well as the main data processing steps. Again, wavelength information is recorded along the columns of the

Biomedical Optics EXPRESS

camera, and the spatial points along the rows. The data is initially acquired as a function of wavelength and then interpolated to wavenumber ($k = 2\pi/\lambda$). To measure B, first we take a Fast Fourier transform (FFT) along the spectral dimension and then filter the resulting peak using a Butterworth filter (this peak corresponds to the optical path length difference between the sample and reference arm, i.e., the first phase argument in Eq. (2)). The filtered signal is transformed back to the spectral domain using an inverse Fourier transform and the phase is extracted for both the test material and solution from which the optical path length difference is calculated, as described by Eq. (3). This process is done for each individual spatial line in the imaging spectrometer, and averaged over 200 central lines. In principle, any part of the image can be used but here we choose the central region as this provides the strongest signal. Finally, by solving Eq. (5) we obtain the concentration independent refractive index increment $B(\lambda)$. Figure 2 illustrated the different steps in data processing.

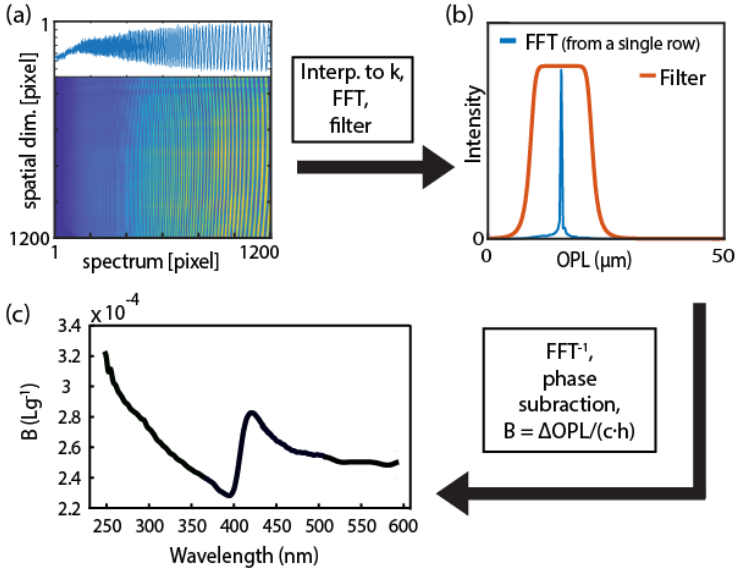

Fig. 2. Different steps in data processing (a) importing interferogram (b) taking fft and filtering (c) calculation of phase difference and dividing by thickness and wavenumber

Random vibrations in the system can introduce an offset in the measured B values (by introducing a random term in L-L'), but the variations do not disturb the spectral features (i.e., its shape). To calibrate the $B(\lambda)$ spectra, we measure the refractive index of the sample and reference solutions at a single wavelength using an Abbe refractometer working at the D-line of sodium (589.6 nm).

To obtain the absorption properties of the sample, we use the independent solvent and sample intensity measurements on the sample arm, and process the data using Beer-Lambert's law:

$$-\ln\left(\frac{I_{sample}}{I_{solvent}}\right) = (\mu_{a-s} + \mu_{a-r})h - (\mu_{a-r})h = \mu_{a-s}h \tag{6}$$

where I_{sample} and $I_{solvent}$ represent the recorded intensities of the test sample and solvent on the sample arm, and $\mu_{a\text{-}s}$ and $\mu_{a\text{-}r}$ are the respective attenuation coefficients. Since $\mu_{a\text{-}s}$ varies with concentration it is desired to convert absorption to an intrinsic material property. To this end, we convert absorption to molar extinction coefficient:

Biomedical Optics EXPRESS

$$\varepsilon(\lambda) = \frac{\mu_{a-s} M}{c \ln(10)} \tag{7}$$

where ε(λ) and M are the molar extinction coefficient and molecular weight, respectively.

4. Results and discussion

Measured molar extinction coefficients and concentration independent refractive index increment spectra within the deep UV to visible range (i.e., 250-600 nm) for all of the tested biochemicals are summarized in Fig. 3 (data are also tabulated in the supplemental materials). The results reveal several important spectral features of the biological materials. For hemoglobin, which we use as reference material since both the absorption and dispersion have been well characterized, our data show the characteristic spectral features, including the Soret peak around 400 nm and the Q bands at 550-600 nm, while the corresponding B(λ) spectrum shows an inverse wavelength-dependence along with the characteristic dispersive 'S'-shape around the Soret peak region and around the Q-bands (a more detailed view is shown in Fig. 5).

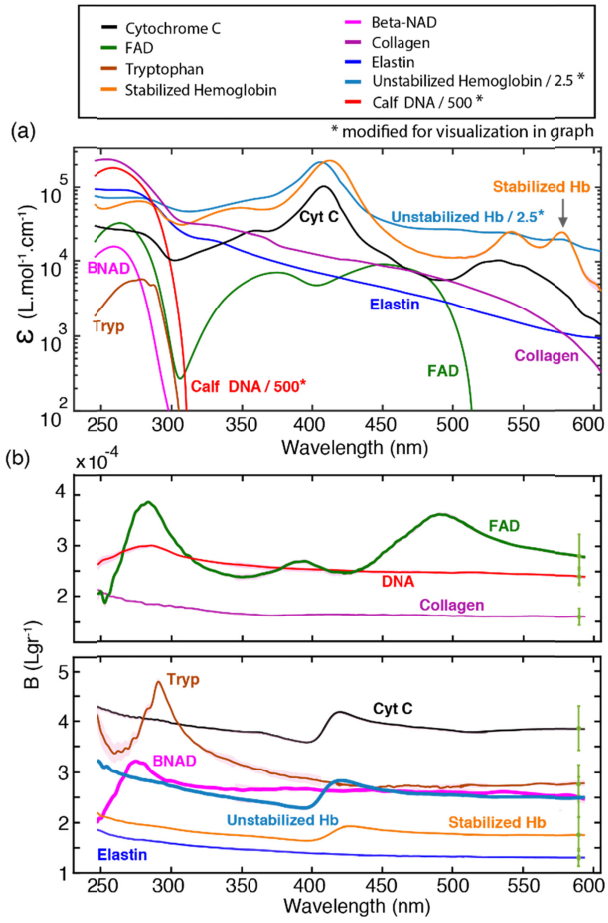

Fig. 3. (a) Measured molar extinction coefficient spectra for tested materials.(See Data File 1 for table of the values) (b) Measured B spectra for tested materials (See Data File 2 for table of the values). To plot all the graphs in a single frame, we have divided Unstabilized Hemoglobin data by 2.5 and Calf DNA data by 500 as stated in the figure. (The supplemental material tabulates the raw data.) B graphs are split for clarity as some curves overlap significantly in certain regions.

Biomedical Optics EXPRESS

Similar characteristics are observed for cytochrome c, which is expected given the shared molecular similarities with hemoglobin [43,44]. DNA, tryptophan, and βNAD show a strong absorption around 260 to 280 nm from nucleic acid and proteins, which is accompanied by a broad dispersive peak in the B(λ) spectra. FAD shows a unique set of three dispersive peaks which roughly trace its corresponding absorption behavior. The green circle located at 589.6 nm shows the calibration point measured with the refractometer. As expected, the corresponding dispersive curves show an overall decreasing B-value with increasing wavelength, and the characteristic 'S'-shape centered about absorptive peaks. Data are also tabulated and available in the supporting materials section. It is worth mentioning that the measured broadband *molar extinction coefficient* spectra are in excellent agreement with values reported in the literature [45–54]. For example, the measured values for aromatic, Soret and Beta band peaks match previously measured values for cytochrome C [45]. Also, for βNAD, the signature adenine peak at 260 nm and lack of protonated nicotinamide (NADH) peak clearly agree with the reported broadband absorption spectrum in [54]. But, again, this is the first time that the dispersive features are reported (with the exception of hemoglobin).

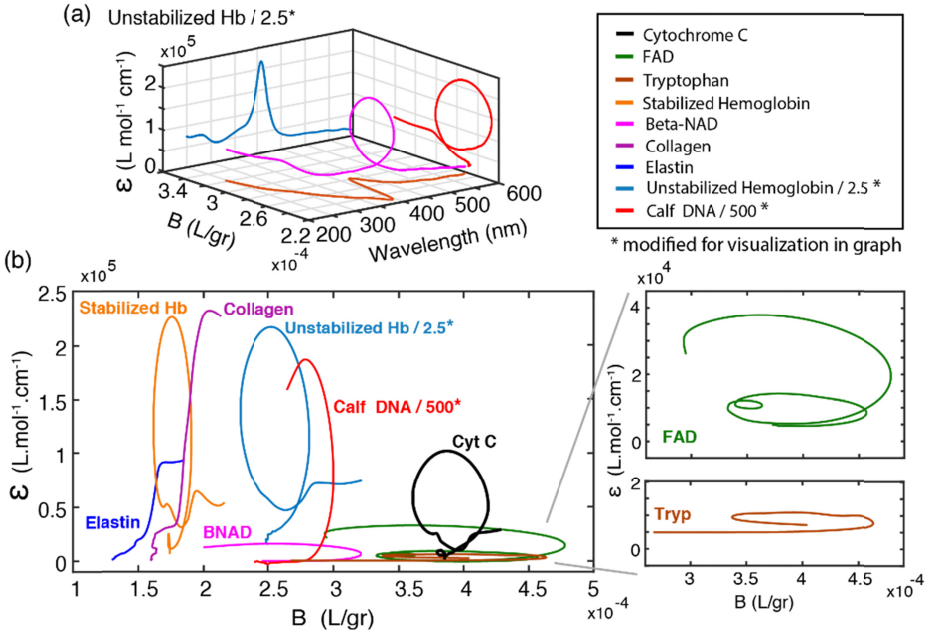

Fig. 4. (a) Projection of ε-B-λ curves on ε-B plane (b) ε-B curves for tested materials, with inset showing magnified ε-B curves for FAD and Tryptophan.

It is also interesting to show B(λ) vs molar extinction coefficient ε(λ) which conveys important information about resonance behavior in these materials, and also represent a different way to potentially distinguish signatures from individual molecules in environments where many molecules are mixed together. To plot B(λ) vs ε(λ), we project the 3D line graphs of B and ε vs wavelength on the B-ε plane (Fig. 4(a)). Figure 4(b) shows the resonance for different materials. One of the most interesting feature in the complex B-ε graphs is that some materials, such as FAD, have multiple resonances (Fig. 4(c)), expressed in the form of a multiple circular paths, while some have no resonance within the range of our study. Representing the data in this fashion provides an additional format to view the complex information and potentially distinguish unique spectral features when many unknown molecules are mixed in cells and/or tissue measurements. This complex plane representation was recently explored for stimulated Raman scattering and was found to be most beneficial

Biomedical Optics EXPRESS

when two or more materials have overlapping or similar absorptive or dispersive properties [55]. Similarly, using the complex plane to represent deep UV absorptive and dispersive properties may enable better differentiation of induvial molecules in a mixture.

An interesting observation about Ferrous stabilized Hemoglobin is that its molar extinction coefficient is almost identical to oxyhemoglobin extracted from red blood cells [45], except for approximately a two-fold difference. (This difference was further validated using a commercial UV-VIS spectrometer). Figure 5(a) shows the molar extinction coefficient for stabilized hemoglobin multiplied by 2.09 along with the values reported in [45]. This multiplicative factor was calculated by least squares fitting. Other small differences include a blueshift in the Soret peak, confirming that the Ferrous stabilized Hb bears some different characteristics from oxy-, deoxy-, and met-Hb as reported in the literature and found inside red blood cells (RBCs) [53,56–58].

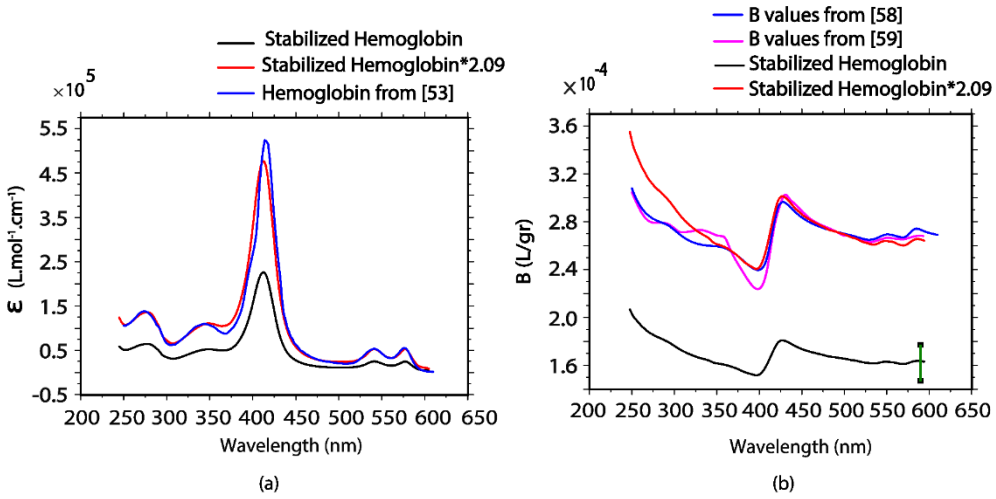

Fig. 5. Comparison of (a) measured molar extinction coefficient of stabilized Hemoglobin in our work and reported by Prahl [45] (b) measured concentration independent refractive index increment of stabilized Hemoglobin and reported data reported by Gienger [59] and Friebel [60].

Careful inspection of the B curves (depicted in Fig. 5(b)) shows differences between the measured B values of stabilized Hb and those previously reported elsewhere in the literature, which again use Hb processed from RBCs [59,60]. However, the calculated least square ratio of the B curves remains the same (2.09), yielding a scaled B spectrum which encompasses the reported values within one standard deviation. It is important to emphasize that while there is a scalar factor difference in the stabilized Hb values used here, the characteristic behavior, including Soret and Q bands, are still clearly observed and follow the behavior of native human Hb.

Another interesting feature observed in the Hb experiments is the effect of UV exposure on the measured spectra. In order to have the best precision and accuracy in our Hemoglobin measurements, it is important to keep UV exposure very short (i.e. in the order of 1 sec.) to avoid unwanted material decomposition and alteration. Thus, a fresh solution is injected on each measurement reported above to ensure that there is no material change and only the primary solution properties are measured. Nevertheless, to illustrate the effect of UV light on Hb, we measured its absorption spectra while being exposed to UV light for 1 minute. The exposure time was set to 75 ms which will produce 800 acquisitions within a minute. For simplicity, the measured spectra are shown in 3.75 second intervals (Fig. 6). By comparing the spectra of the first and last acquisitions, it is evident that the spectrum is evolving from that of oxy-Hb to a spectrum that represents the spectral features of methemoglobin [58],

Biomedical Optics EXPRESS

confirming that the Fe^{2+} (ferrous) ion in the heme groups are changing to Fe^{3+}(ferric) under UV illumination due to its high oxidation potency [61–64]. Such temporal dynamics were not observed in any of the other molecules tested in this study.

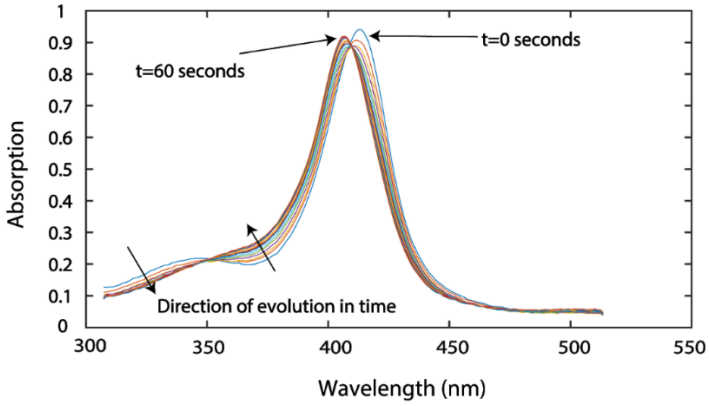

Fig. 6. Variation of absorption in stabilized Hemoglobin exposed to Eq. (-99)X broadband source within 1 minute.

Since Ultraviolet hyperspectral interferometry (UHI) microscopy is capable of imaging and quantifying absorptive and dispersive properties of biological materials [1], it is important to understand the concentration detection limits of our system based on the measured ε and B, and compare them to expected physiologically relevant concentrations in human cells and tissues. To this end, the standard deviation in optical pathlength difference and absorption is calculated and attributed to detection limit of each tested material and compared against their physiological concentrations in cells or tissues. To calculate the detection limits we use the highest values (highest detection limit wavelength) for B and ε within the measurement range and then calculate the detection limit for the concentration using Eqs. (5) and (7). The results are summarized in Table 2.

Table 2. Calculated detection limits based on B and ε for each biological material. Typical concentration of each biochemical in human body is listed for comparison.

Chemical name	Concentration detection limit per millimeter using B (gr/L-mm)	Concentration detection limit per millimeter using ε (gr/L-mm)	Concentration in human body per millimeter (gr/L-mm)
Hemoglobin	6.358×10^{-3}	4.62×10^{-5}	0.825 (human red blood cell) [56,65,66]
β-Nicotinamide adenine dinucleotide	3.366×10^{-3}	3.63×10^{-4}	2.74×10^{-3} –6.854×10^{-3} (for typical mammalian cell [67]
Flavin adenine dinucleotide	2.64×10^{-3}	2.2×10^{-4}	1.43×10^{-3} (for human breast cell) [68]
Tryptophan	4.84×10^{-3}	3.52×10^{-4}	0.013 human serum [69]
Cytochrome C	3.652×10^{-3}	1.32×10^{-3}	0.167-0.245 (for Cardiomyocytes cells) [70,71]
Collagen	3.806×10^{-3}	5.06×10^{-3}	7344 (human skin) [72–74]
Calf thyme DNA	7.04×10^{-3}	7.7×10^{-4}	0.12-0.248 [75,76]
Elastin	9.68×10^{-3}	6.16×10^{-3}	408 [77] (human skin)

It is evident that the calculated detection limits using our system are below the typical concentrations of biological materials in human tissue or cells, implying they are indeed detectable. This is important as it further supports the notion that UV spectral imaging can

Biomedical Optics EXPRESS

provide highly specific information of multiple endogenous biochemicals for molecular imaging. We also note that the detection limits calculated from absorption are lower than its dispersive counterpart. This may be attributed to instabilities in this interferometic set up in which no individual measurement contains a background reference region. Such instabilities can be more effectively eliminated when imaging since a background region can be used as reference. Another potential reason why absorption provides a slightly lower (better) detection limits is that the attenuation here is calculated from separate measurements of the sample are reference arms, which gives a factor of two improvement in sensitivity as compared to using the interference term.

Finally, it is important to emphasize that for each material we tested several concentrations and calculated their corresponding molar extinction coefficient and concentration independent refractive index increment values and observed consistent results. In addition, to test the uniformity of the sample, we collected data from various regions of the flow cell and again obtained consistent results.

5. Conclusion

In conclusion, we have used an interferometric approach to measure intrinsic absorptive and dispersive properties of biomolecules in the deep-UV-Vis region of the spectrum. This information can be used to help identify these biomolecules and determine their concentration in thin tissue samples or individual cells. Our results reveal characteristic footprints of these biomolecules for both absorption and dispersion in the 250 to 590 nm region of spectrum. Data are tabulated in supplemental materials. The materials tested in our experiments are important materials in the human body that promote metabolism, biosynthesis and hormone balance. The detection limit analysis shows that this system is capable of distinguishing these molecules at physiologically relevant concentrations. The natural levels of these materials change due to disease, including cancer, and therefore detection, characterization and monitoring these biomaterials is important. These results can, for example, help better characterize/phenotype thin biopsy tissue samples or live and fixed cells for various biomedical applications. This work further supports the potential of deep-UV spectroscopy for highly sensitive, label-free molecular imaging.

Funding

National Science Foundation (NSF CBET CAREER 1752011); Burroughs Welcome Fund (CASI BWF1014540); Galloway Foundation and Integrated Cancer Research Center, Georgia Institute of Technology.

Acknowledgments

We appreciate all the efforts and useful help from Keya Patel and Amy Azad. We would also like to appreciate all help and support we received from Dr. Amanda B. Stephens and Dr. Hui Zhu from the Department of Chemistry at Georgia Institute of Technology.

Disclosures

The authors declare that there are no conflicts of interest related to this article.

References

1. A. Ojaghi, M. E. Fay, W. A. Lam, and F. E. Robles, "Ultraviolet Hyperspectral Interferometric Microscopy," Sci. Rep. **8**(1), 9913 (2018).
2. F. E. Robles, L. L. Satterwhite, and A. Wax, "Nonlinear phase dispersion spectroscopy," Opt. Lett. **36**(23), 4665–4667 (2011).
3. C. Yang, A. Wax, I. Georgakoudi, E. B. Hanlon, K. Badizadegan, R. R. Dasari, and M. S. Feld, "Interferometric phase-dispersion microscopy," Opt. Lett. **25**(20), 1526–1528 (2000).
4. P. Hlubina, J. Luňáček, D. Ciprian, and R. Chlebus, "Spectral interferometry and reflectometry used to measure thin films," Appl. Phys. B **92**(2), 203–207 (2008).

Biomedical Optics EXPRESS

5. J. Jung, K. Kim, J. Yoon, and Y. Park, "Hyperspectral optical diffraction tomography," Opt. Express **24**(3), 2006–2012 (2016).
6. Y. Park, T. Yamauchi, W. Choi, R. Dasari, and M. S. Feld, "Spectroscopic phase microscopy for quantifying hemoglobin concentrations in intact red blood cells," Opt. Lett. **34**(23), 3668–3670 (2009).
7. K. Lee, K. Kim, J. Jung, J. Heo, S. Cho, S. Lee, G. Chang, Y. Jo, H. Park, and Y. Park, "Quantitative phase imaging techniques for the study of cell pathophysiology: from principles to applications," Sensors (Basel) **13**(4), 4170–4191 (2013).
8. K. Creath and G. Goldstein, "Dynamic quantitative phase imaging for biological objects using a pixelated phase mask," Biomed. Opt. Express **3**(11), 2866–2880 (2012).
9. K. Lee, Y. Kim, J. Jung, H. Ihee, and Y. Park, "Measurements of complex refractive index change of photoactive yellow protein over a wide wavelength range using hyperspectral quantitative phase imaging," Sci. Rep. **8**(1), 3064 (2018).
10. K. Itoh, T. Inoue, T. Yoshida, and Y. Ichioka, "Interferometric supermultispectral imaging," Appl. Opt. **29**(11), 1625–1630 (1990).
11. I. Kassamakov, S. Lecler, A. Nolvi, A. Leong-Hoï, P. Montgomery, and E. Hæggström, "3D Super-Resolution Optical Profiling Using Microsphere Enhanced Mirau Interferometry," Sci. Rep. **7**(1), 3683 (2017).
12. H. Ooki, Y. Iwasaki, and J. Iwasaki, "Differential interference contrast microscope with differential detection for optimizing image contrast," Appl. Opt. **35**(13), 2230–2234 (1996).
13. M. R. Arnison, K. G. Larkin, C. J. R. Sheppard, N. I. Smith, and C. J. Cogswell, "Linear phase imaging using differential interference contrast microscopy," J. Microsc. **214**(Pt 1), 7–12 (2004).
14. F. E. Robles and A. Wax, "Separating the scattering and absorption coefficients using the real and imaginary parts of the refractive index with low-coherence interferometry," Opt. Lett. **35**(17), 2843–2845 (2010).
15. F. E. Robles, S. Chowdhury, and A. Wax, "Assessing hemoglobin concentration using spectroscopic optical coherence tomography for feasibility of tissue diagnostics," Biomed. Opt. Express **1**(1), 310–317 (2010).
16. F. M. Hoffmann, "Infrared reflection-absorption spectroscopy of adsorbed molecules," Surf. Sci. Rep. **3**(2-3), 107–192 (1983).
17. M. Manley, "Near-infrared spectroscopy and hyperspectral imaging: non-destructive analysis of biological materials," Chem. Soc. Rev. **43**(24), 8200–8214 (2014).
18. A. M. Katzenmeyer, G. Holland, K. Kjoller, and A. Centrone, "Absorption spectroscopy and imaging from the visible through mid-infrared with 20 nm resolution," Anal. Chem. **87**(6), 3154–3159 (2015).
19. M. Pilling and P. Gardner, "Fundamental developments in infrared spectroscopic imaging for biomedical applications," Chem. Soc. Rev. **45**(7), 1935–1957 (2016).
20. S. Arora, J. Mauser, D. Chakrabarti, and A. Schulte, "Spatially resolved micro-absorption spectroscopy with a broadband source and confocal detection," Opt. Commun. **355**, 533–537 (2015).
21. F. Siti Sakinah Mohd, N. Suardi, and I. S. Mustafa, "In Vitro UV-Visible Spectroscopy Study of Yellow Laser Irradiation on Human Blood," J. Phys. Conf. Ser. **995**, 012053 (2018).
22. D. A. Proshlyakov, "UV optical absorption by protein radicals in cytochrome c oxidase," Biochim. Biophys. Acta **1655**(1-3), 282–289 (2004).
23. H. R. Thapa, A. J. Lail, N. Garg, and V. Agarwal, "Chapter Ten - Chemoenzymatic Synthesis of Starting Materials and Characterization of Halogenases Requiring Acyl Carrier Protein-Tethered Substrates," in *Methods in Enzymology*, B. S. Moore, ed. (Academic Press, 2018), pp. 333–366.
24. L. G. Whitby, "A new method for preparing flavin-adenine dinucleotide," Biochem. J. **54**(3), 437–442 (1953).
25. X. Ma, L. Li, C. Xu, H. Wei, X. Wang, and X. Yang, "Spectroscopy and speciation studies on the interactions of aluminum (III) with ciprofloxacin and β-nicotinamide adenine dinucleotide phosphate in aqueous solutions," Molecules **17**(8), 9379–9396 (2012).
26. C. S. Thom, C. F. Dickson, D. A. Gell, and M. J. Weiss, "Hemoglobin variants: biochemical properties and clinical correlates," Cold Spring Harb. Perspect. Med. **3**(3), a011858 (2013).
27. P. Belenky, K. L. Bogan, and C. Brenner, "NAD+ metabolism in health and disease," Trends Biochem. Sci. **32**(1), 12–19 (2007).
28. M. Ziegler, "New functions of a long-known molecule. Emerging roles of NAD in cellular signaling," Eur. J. Biochem. **267**(6), 1550–1564 (2000).
29. M. Barile, T. A. Giancaspero, C. Brizio, C. Panebianco, C. Indiveri, M. Galluccio, L. Vergani, I. Eberini, and E. Gianazza, "Biosynthesis of flavin cofactors in man: implications in health and disease," Curr. Pharm. Des. **19**(14), 2649–2675 (2013).
30. G. Kuppuraj, D. Kruise, and K. Yura, "Conformational behavior of flavin adenine dinucleotide: conserved stereochemistry in bound and free states," J. Phys. Chem. B **118**(47), 13486–13497 (2014).
31. J. H. Kristensen and M. A. Karsdal, "Chapter 30 - Elastin," in *Biochemistry of Collagens, Laminins and Elastin*, M. A. Karsdal, ed. (Academic Press, 2016), pp. 197–201.
32. E. Margoliash, "Primary structure and evolution of cytochrome C," Proc. Natl. Acad. Sci. U.S.A. **50**(4), 672–679 (1963).
33. X. Liu, C. N. Kim, J. Yang, R. Jemmerson, and X. Wang, "Induction of apoptotic program in cell-free extracts: requirement for dATP and cytochrome c," Cell **86**(1), 147–157 (1996).
34. R. K. Gupta, R. Pandey, G. Sharma, R. Prasad, B. Koch, S. Srikrishna, P.-Z. Li, Q. Xu, and D. S. Pandey, "DNA binding and anti-cancer activity of redox-active heteroleptic piano-stool Ru(II), Rh(III), and Ir(III) complexes containing 4-(2-methoxypyridyl)phenyldipyrromethene," Inorg. Chem. **52**(7), 3687–3698 (2013).

Biomedical Optics EXPRESS

35. L. Shivakumar, K. Shivaprasad, and H. D. Revanasiddappa, "SODs, DNA binding and cleavage studies of new Mn(III) complexes with 2-((3-(benzyloxy)pyridin-2-ylimino)methyl)phenol," Spectrochim. Acta A Mol. Biomol. Spectrosc. **107**, 203–212 (2013).
36. J. L. García-Giménez, J. Hernández-Gil, A. Martínez-Ruíz, A. Castiñeiras, M. Liu-González, F. V. Pallardó, J. Borrás, and G. Alzuet Piña, "DNA binding, nuclease activity, DNA photocleavage and cytotoxic properties of Cu(II) complexes of N-substituted sulfonamides," J. Inorg. Biochem. **121**, 167–178 (2013).
37. A. Slominski, I. Semak, A. Pisarchik, T. Sweatman, A. Szczesniewski, and J. Wortsman, "Conversion of L-tryptophan to serotonin and melatonin in human melanoma cells," FEBS Lett. **511**(1-3), 102–106 (2002).
38. J. D. Schaechter and R. J. Wurtman, "Serotonin release varies with brain tryptophan levels," Brain Res. **532**(1-2), 203–210 (1990).
39. L. Bozec, G. van der Heijden, and M. Horton, "Collagen fibrils: nanoscale ropes," Biophys. J. **92**(1), 70–75 (2007).
40. L. J. Gould, "Topical collagen-based biomaterials for chronic wounds: rationale and clinical application," Adv. Wound Care **5**(1), 19–31 (2016).
41. A. Daneault, "Hydrolyzed collagen contributes to osteoblast differentiation in vitro and subsequent bone health in vivo," Osteoarthritis Cartilage **22**, S131 (2014).
42. A. Daneault, J. Prawitt, V. Fabien Soulé, V. Coxam, and Y. Wittrant, "Biological effect of hydrolyzed collagen on bone metabolism," Crit. Rev. Food Sci. Nutr. **57**(9), 1922–1937 (2017).
43. S. E. J. Bowman and K. L. Bren, "The chemistry and biochemistry of heme C: functional bases for covalent attachment," Nat. Prod. Rep. **25**(6), 1118–1130 (2008).
44. R. V. Chertkova, N. A. Brazhe, T. V. Bryantseva, A. N. Nekrasov, D. A. Dolgikh, A. I. Yusipovich, O. Sosnovtseva, G. V. Maksimov, A. B. Rubin, and M. P. Kirpichnikov, "New insight into the mechanism of mitochondrial cytochrome c function," PLoS One **12**(5), e0178280 (2017).
45. R. R. R. Sardari, S. R. Zarchi, S. Hajihosseini, Z. Aghili, R. Rasoolzadeh, S. Imani, H. Borna, A. M. Zand, A. Nejadmoghadam, M. Ghalavand, and Y. Panahi, "Identification of an independent measurement method for denaturation studies of cytochrome C," Int. J. Electrochem. Sci. **8**, 11578–11587 (2013).
46. F. Zhang, A. Wang, Z. Li, S. He, and L. Shao, "Preparation and Characterisation of Collagen from Freshwater Fish Scales," Food Nutr. Sci. **2**(08), 818 (2011).
47. T. Mitra, P. J. Manna, S. T. K. Raja, A. Gnanamani, and P. P. Kundu, "Curcumin loaded nano graphene oxide reinforced fish scale collagen – a 3D scaffold biomaterial for wound healing applications," RSC Advances **5**(119), 98653–98665 (2015).
48. D. Joshi, D. Kumar, A. K. Maini, and R. C. Sharma, "Detection of biological warfare agents using ultra violet-laser induced fluorescence LIDAR," Spectrochim. Acta A Mol. Biomol. Spectrosc. **112**, 446–456 (2013).
49. C. K. Mathews, K. E. Van Holde, D. R. Appling, and S. J. Anthony-Cahill, *Biochemistry* (Pearson, Toronto, 2013).
50. G. Javier, S.-V. Isabel, N. Jesús, and M. Susana de, "The intrinsic fluorescence of FAD and its application in analytical chemistry: a review," Methods Appl. Fluoresc. **4**, 042005 (2016).
51. L. Valle, I. Abatedaga, F. E. M. Vieyra, A. Bortolotti, N. Cortez, and C. D. Borsarelli, "Enhancement of photophysical and photosensitizing properties of flavin adenine dinucleotide by mutagenesis of the C-terminal extension of a bacterial flavodoxin reductase," ChemPhysChem **16**(4), 872–883 (2015).
52. K. R. Millington, "Diffuse reflectance spectroscopy of fibrous proteins," Amino Acids **43**(3), 1277–1285 (2012).
53. J. Y. Lo, J. Q. Brown, S. Dhar, B. Yu, G. M. Palmer, N. M. Jokerst, and N. Ramanujam, "Wavelength optimization for quantitative spectral imaging of breast tumor margins," PLoS One **8**(4), e61767 (2013).
54. R. M. C. Dawson, *Data for Biochemical Research,* 3rd ed. ed. (Clarendon Press, Oxford, 1986).
55. V. Kumar, A. D. Cadena, A. Perri, F. Preda, N. Coluccelli, G. Cerullo, and D. Polli, "Invited Article: Complex vibrational susceptibility by interferometric Fourier transform stimulated Raman scattering," APL Photonics **3**(9), 092403 (2018).
56. G. Zonios, L. T. Perelman, V. Backman, R. Manoharan, M. Fitzmaurice, J. Van Dam, and M. S. Feld, "Diffuse reflectance spectroscopy of human adenomatous colon polyps in vivo," Appl. Opt. **38**(31), 6628–6637 (1999).
57. H. Zhu, D. Li, M. Liu, V. Copié, and B. Lei, "Non-heme-binding domains and segments of the Staphylococcus aureus IsdB protein critically contribute to the kinetics and equilibrium of heme acquisition from methemoglobin," PLoS One **9**(6), e100744 (2014).
58. R. Deshmukh and V. Trivedi, "Pro-stimulatory role of methemoglobin in inflammation through hemin oxidation and polymerization," Inflamm. Allergy Drug Targets **12**(1), 68–78 (2013).
59. J. Gienger, H. Groß, J. Neukammer, and M. Bär, "Determining the refractive index of human hemoglobin solutions by Kramers-Kronig relations with an improved absorption model," Appl. Opt. **55**(31), 8951–8961 (2016).
60. M. Friebel and M. Meinke, "Model function to calculate the refractive index of native hemoglobin in the wavelength range of 250-1100 nm dependent on concentration," Appl. Opt. **45**(12), 2838–2842 (2006).
61. E. J. Benz and B. L. Ebert, "Chapter 43 - Hemoglobin Variants Associated With Hemolytic Anemia, Altered Oxygen Affinity, and Methemoglobinemias," in *Hematology (Seventh Edition)*, R. Hoffman, E. J. Benz, L. E. Silberstein, H. E. Heslop, J. I. Weitz, J. Anastasi, M. E. Salama, and S. A. Abutalib, eds. (Elsevier, 2018), pp. 608–615.
62. J. D. Belcher, J. D. Beckman, G. Balla, J. Balla, and G. Vercellotti, "Heme degradation and vascular injury," Antioxid. Redox Signal. **12**(2), 233–248 (2010).

Biomedical Optics EXPRESS

63. M. F. Holick, "Biological effects of sunlight, ultraviolet radiation, visible light, infrared radiation and vitamin D for health," Anticancer Res. **36**(3), 1345–1356 (2016).
64. L. Pan, X. Wang, S. Yang, X. Wu, I. Lee, X. Zhang, R. A. Rupp, and J. Xu, "Ultraviolet irradiation-dependent fluorescence enhancement of hemoglobin catalyzed by reactive oxygen species," PLoS One **7**(8), e44142 (2012).
65. A. M. Stadler, I. Digel, G. M. Artmann, J. P. Embs, G. Zaccai, and G. Büldt, "Hemoglobin dynamics in red blood cells: correlation to body temperature," Biophys. J. **95**(11), 5449–5461 (2008).
66. S. Krueger and R. Nossal, "SANS studies of interacting hemoglobin in intact erythrocytes," Biophys. J. **53**(1), 97–105 (1988).
67. Y. Yang and A. A. Sauve, "NAD+ metabolism: Bioenergetics, signaling and manipulation for therapy," Biochim. Biophys. Acta **1864**(12), 1787–1800 (2016).
68. A. T. Lutes, "Intrinsic flavin as a biomarker for monitoring pathologically-induced changes in cellular energy metabolism," Thesis: The Pennsylvania State University (2008).
69. S. Comai, A. Bertazzo, N. Carretti, A. Podfigurna-Stopa, S. Luisi, and C. V. L. Costa, "Serum levels of tryptophan, 5-hydroxytryptophan and serotonin in patients affected with different forms of amenorrhea," Int. J. Tryptophan Res. **3**, 69–75 (2010).
70. B. J. van Beek-Harmsen and W. J. van der Laarse, "Immunohistochemical determination of cytosolic cytochrome C concentration in cardiomyocytes," J. Histochem. Cytochem. **53**(7), 803–807 (2005).
71. R. E. Tracy and G. E. Sander, "Histologically measured cardiomyocyte hypertrophy correlates with body height as strongly as with body mass index," Cardiol. Res. Pract. **2011**, 658958 (2011).
72. R. E. Neuman and M. A. Logan, "The determination of collagen and elastin in tissues," J. Biol. Chem. **186**(2), 549–556 (1950).
73. T. Igarashi, K. Nishino, and S. K. Nayar, "The Appearance of Human Skin: A Survey," Found. Trends Comput. Graph. Vis. **3**(1), 1–95 (2007).
74. X. Liang and S. A. Boppart, "Biomechanical properties of in vivo human skin from dynamic optical coherence elastography," IEEE Trans. Biomed. Eng. **57**(4), 953–959 (2010).
75. B. J. Zeskind, "Quantitative imaging of living cells by deep ultraviolet microscopy," Thesis (Ph. D., Massachusetts Institute of Technology, Biological Engineering Division (2006).
76. A. Gualberto, R. M. Patrick, and K. Walsh, "Nucleic acid specificity of a vertebrate telomere-binding protein: evidence for G-G base pair recognition at the core-binding site," Genes Dev. **6**(5), 815–824 (1992).
77. E. Shiratsuchi, M. Nakaba, and M. Yamada, "Elastin hydrolysate derived from fish enhances proliferation of human skin fibroblasts and elastin synthesis in human skin fibroblasts and improves the skin conditions," J. Sci. Food Agric. **96**(5), 1672–1677 (2016).